DC/AC/RF Characteristics of Multi-Channel GAA NS FETs with ML and BL MoS_2

Yueh-Ju Chan
Institute of Communications Engineering and
Parallel and Scientific Computing Laboratory
National Yang Ming Chiao Tung Univeristy
Hsinchu 300093, Taiwan.
yjchan@mail.ymlab.org

Sekhar Reddy Kola
EECS International Graduate Program and
Parallel and Scientific Computing Laboratory
National Yang Ming Chiao Tung Univeristy
Hsinchu 300093, Taiwan
sekhar.kola@mail.ymlab.org

Yiming Li
Institue of Communications Engineering and
Parallel and Scientific Computing Laboratory
National Yang Ming Chiao Tung Univeristy
Hsinchu 300093, Taiwan
ymli@mail.ymlab.org

***Abstract*—For the first time, we examine the performance of gate-all-around nanosheet field effect transistor (GAA NS FET) with both monolayer (ML) and bilayer (BL) molybdenum disulfide (MoS_2). As compared to the control sample of silicon (Si), MoS_2 devices exhibit reduced short-channel effects (SCE) owing to its larger band gap and larger effective mass. The GAA NS FET with BL MoS_2 possesses moderate energy bandgap and large channel thickness which exhibits superior on state current and voltage gain.**

***Keywords*—GAA NS FETs, BL and ML MoS_2, electronic properties, DC/AC/RF characteristics.**

I. Introduction

In recent years, transition metal dichalcogenides (TMDCs) have gained considerable attention due to their 2D properties and reasonable energy bandgaps. It has been found that MoS_2 belongs to the TMDC family with an indirect bandgap of 1.2 eV in bulk, while performing direct bandgap of 1.8 eV in monolayer [1]-[2]. MoS_2 exhibits low mobility when it is deposited on SiO_2; however, when it is deposited on HfO_2 as the oxide of the transistor, it exhibits a higher mobility of 217 $cm^2V^{-1}s^{-1}$ [3]. In contrast to Si nanodevices, which suffers from serious SCEs, MoS_2 devices may have superior electrical properties and have been studied as potential candidates for advanced CMOS technologies [4]-[5]; nonetheless, the results are still limited to reach the requirement to sub-10 nm and high on/off ratio simultaneously. Computationally, device simulation by using the density functional theory (DFT) and the nonequilibrium Green's function (NEGF) [6] can provide the most accurate results; however, huge computational resources are required for complicated cases. Thus, integrating key result of DFT calculation into a conventional device simulation, after careful calibration with the results of DFT and NEGF, enables us to explore 3D devices effectively [7].

In this study, based on a properly calibrated device simulation with the results of DFT and NEGF, we first explore GAA NS FET with ML and BL MoS_2 films, where the calibrated bandgap, electron affinity, and effective mass of MoS_2 are then incorporated into device simulation to explore DC/AC/RF characteristics of a three-channel GAA NS FET.

II. Device Simulation of GAA NS FET MoS_2

For the GAA NS FET in Fig. 1(a), the ML and BL MoS_2 channels are shows in Fig. 1(b). The cut c_1 plane of the device is shown in Fig. 1(c) with a 0.6-nm SiO_2 at the inner layer and a 2-nm HfO_2 at the outer layer. The first-principle simulations of ML and BL MoS_2, via QuantumATK [8], lie in the first Brillouin zone of ΓMKΓ, as shown in Fig. 1(d). The DFT calculations are with the Perdew-Burke-Ernzerhof (PBE) and generalized gradient approximation (GGA) functionals. The k point sampling of ML and BL MoS_2 is 10×10×1 and 10×10×2, respectively, with a 1.5-nm vacuum layer for the relaxation. A simulation of the band structure is then conducted for the

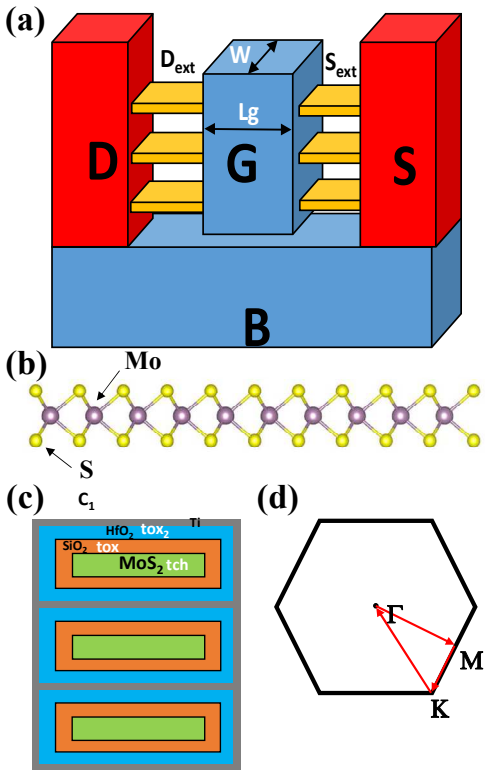

Fig. 1. (a) A 3D schematic diagram of the three-channel GAA NS FET using silicon (t_{ch} = 5 nm), ML MoS_2 (t_{ch} = 0.65 nm), and MoS_2 BL (t_{ch} = 1.4 nm) as its channel, respectively. (b) The schematic plot of ML MoS_2 using as channel. (c) The cut-c_1 plane in GAA NS FET (d) The first Brillouin zone of MoS_2.

bandgap, effective mass, and density-of-states (DOS) of the electron affinity. Then, we plug the calculated electronic structures of MoS_2 into a density gradient based quantum-corrected 3D drift-diffusion simulation to study device characteristics of GAA NS FETs. The channel thickness of ML and BL MoS_2, and Si are 0.65, 1.4, and 5 nm, respectively. A high-field transport mobility based on Caughey-Thomas formula for the scattering is adopted. For electrons in ML MoS_2, the saturation velocity is given by $v_d = \mu_{LF}F/(1 + (\mu_{LF}F/v_{sat})^{\gamma})^{\gamma}$, where the low-field mobility $\mu_{LF} \equiv (\partial v_d/\partial F)|_{F\to 0} \approx 36.7$ $cm^2/V^{-1}s^{-1}$ and $\gamma \approx 2.8$ [9]. For the recombination and generation, we use the Schottky Read Hall and Auger models based on fabricated MoS_2 devices [10]. Details of device settings are listed in Tab. I.

III. Results and Discussion

MoS_2 Brillouin zone is illustrated in Fig. 1(d). We calculate the band structure along ΓMKΓ in the first Brillouin zone. The results of band structure are shown in Figs. 3(a)-(c).In ML MoS_2, it exhibits a direct bandgap of 1.78 eV. In BL MoS_2, however, shows an indirect bandgap of 1.40 eV. This can be explained by the fact that Γ point of the valence band

TABLE I LIST OF THE ADOPTED PARAMETERS IN THE DEVICE SIMULATION OF GAA NS FETS. IT INCLUDES THE GATE LENGTH L_G, THE OXIDE THICKNESS T_{OX} FOR SiO_2, THE T_{OX2} FOR HfO_2, AND THE CHANNEL DOPING PROFILE.

Parameters	Numeric Values
L_g (nm)	6 ~ 16
W (nm)	10
t_{ch} (nm)	0.65
t_{ox} (nm)	0.6
t_{ox2} (nm)	2
EOT (nm)	0.96
Channel Doping (cm^{-3})	$5 X10^{17}$
S/D Doping (cm^{-3})	$1X10^{20}$
S_{ext}/D_{ext} Doping (cm^{-3})	$1.2X10^{19}$

Steps of Simulation and Calibration

Step 1: DFT calculations for the bandgap, effective Mass, and electron Affinity.

Step 2: Device simulation by numerically solving a set of density gradient based quantum-corrected 3D drift-diffusion equations.

Step 3: Calibration of the device simulation with the results of NEGF simulation for the accuracy tuning.

Step 4: Apply the validated device simulation for the multi-channel GAA NS FETs with ML and BL MoS_2.

Fig. 2. A workflow of the adopted device simulation process.

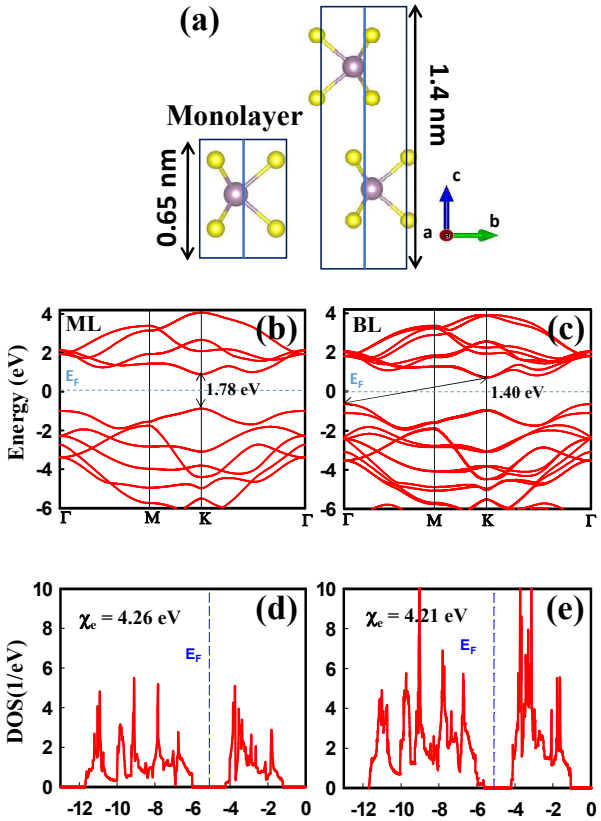

Fig. 3. (a) Schematic diagram of the ML and BL MoS_2 structures. The thicknesses of ML and BL are 0.65 and 1.4 nm, respectively. The simulated values of band gap E_g = 1.78 and 1.40 eV are for the (b) ML and (c) BL, respectively. (d) Plots of the DOS using absolute energy as the zero point of the eV for simulating the electron affinity of ML and (e) BL, where the calculated values of electron affinity (χ_e) are 4.26 and 4.21 eV in the ML and BL, respectively.

maximum (VBM) in BL MoS_2 has shifted to a higher value than K point, while stays at lower value in ML MoS_2. The K point is chosen as the symmetric point of conduction band minimum (CBM) in both ML and BL calculations of the electron effective mass. The simulated effective mass in BL

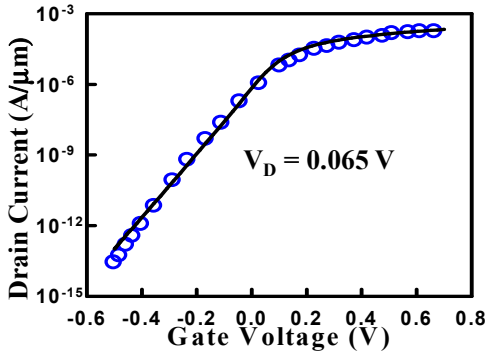

Fig. 4. The calibrated I_D-V_G curves of the N-type MoS_2 device between the adopted device and NEGF simulations.

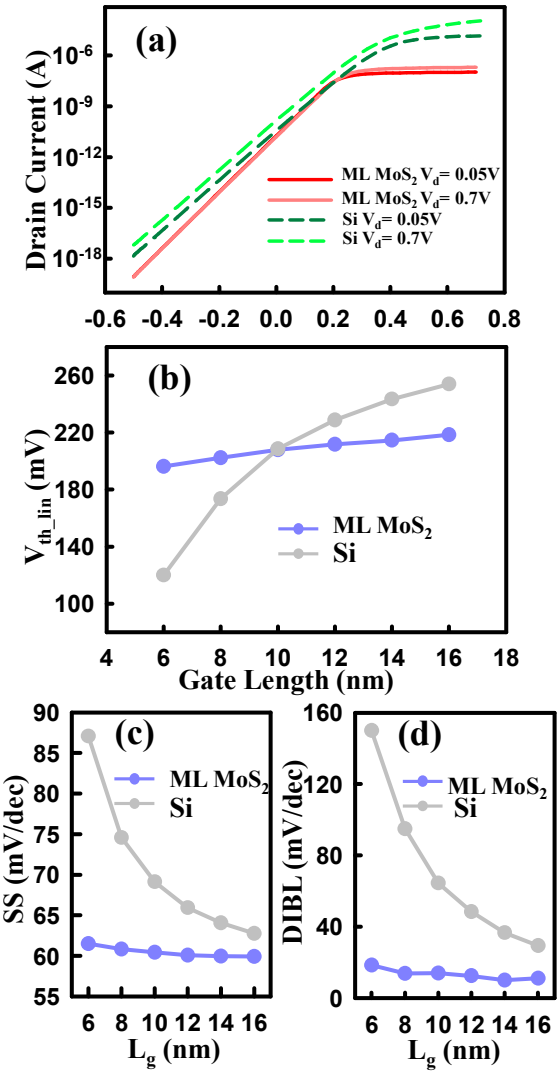

Fig. 5. (a) The transfer characteristic of the 10-nm ML MoS_2 GAA NS FET, compared with the Si one. (b) A comparison of the V_{th} roll-off between the ML MoS_2 and Si devices. The variation of the (c) subthreshold swing (SS) and (d) drain-induced barrier lowing (DIBL) with respect to the gate length (L_G).

MoS_2 is larger than that in ML MoS_2, the results perform $0.608m_0^*$ in BL, whereas $0.456m_0^*$ in ML. According to Figs. 3(d)-(e), the electron affinity of both cases is nearly identical with marginal differences between them. As the results, for ML and BL, the values are 0.426 and 0.421, respectively. The calculated results compared with different theoretical results [1], [7], [12]-[16] are listed in Tab. II; they are revealed that

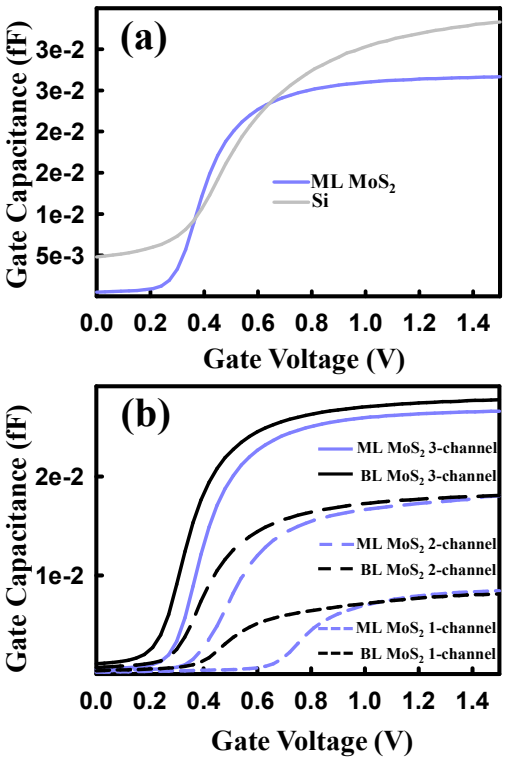

Fig. 6. (a) The C_g-V_g curves comparing with ML MoS_2 and Si. (b) The C_g-V_g curves of the ML and BL MoS_2 GAA NS FETs at L_g = 10 nm.

the results are in engineering reasonable values for further device simulation. According to the results of DFT, a proper calibration of the quantum mechanically corrected device simulation with the simulation of NEGF is performed, as shown in Fig. 4 at V_{ds} = 0.065 V. The simulated results of transfer curve turns out to fit in the NEGF method well.

We do further use the validated device simulation results for the multi-channel GAA NS FET with ML/BL MoS_2 and Si. The results are shown in Fig. 5. Due to the larger channel thickness (t_{ch}) and the greater mobility of Si, the I_{on} of Si are larger than MoS_2 shown in Fig. 5(a). However, after we extract the linear threshold voltage (V_{th_lin}) at 206 mV in both Si and ML MoS_2 devices at the gate length (L_g) in 10 nm in Fig. 5(b). As the L_g value is increased from 6 to 16 nm, due to the 2D t_{ch} of MoS_2 with larger bandgap as well as larger m_0^*, the SS and DIBL are remaining stable in the ML MoS_2 cases while showing strong degradation in Si in Figs. 5(c) and (d), respectively. The degradation ratios (38.7% and 410.5%, respectively) are revealed in Si, meanwhile remains sustainable with low degradation ratio (7.7% in SS and 39.9% in DIBL) in ML MoS_2.

Figure 6(a) shows the gate capacitance versus gate voltage (C_g-V_g) curves of the explored devices, where C_g in Si is mainly due to the oxide layer, whereas C_g in MoS_2 is due to t_{ch}. C_g in Si device is 19.6% larger than ML MoS_2, which means that MoS_2 could have better performance comparing with Si in GAA NS devices due to larger gate capacitance cause larger power consumption in Si device. C_g-V_g curves with number of channels in ML and BL MoS_2 is shown in Fig. 6(b). As channel number increases, the value of C_g enhances; besides, the shift of C_g between ML and BL MoS_2 in 3-channel is smaller than that of 2- and 1-channel. These results are due to the effective channel area in 3-channel becomes larger, which makes the effect of 2-channel and 1-channel turn out to become smaller.

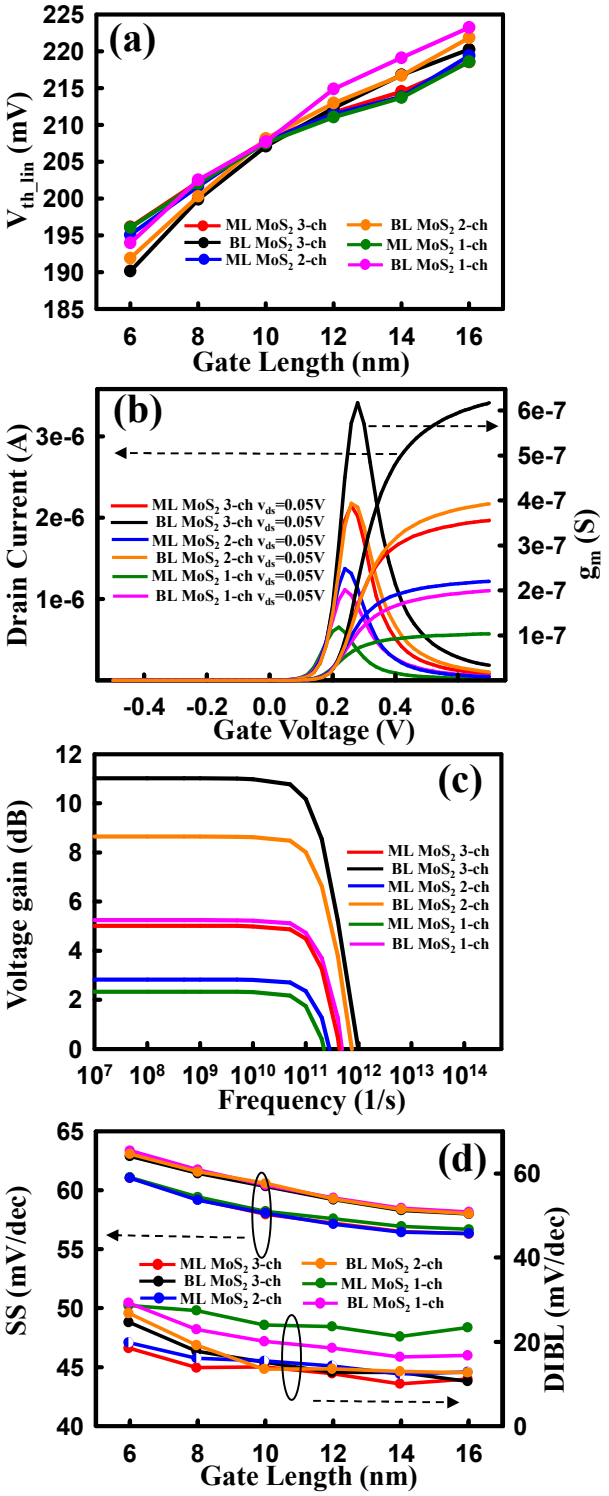

Fig. 7. (a) I_d-V_g curves compared with ML and BL MoS_2 in linear region (V_d = 0.05 V) (b) The V_{th} of ML and BL MoS_2. (c) The DIBL and of ML and BL MoS_2 with varied L_g. (d) The Bode plot of ML and BL MoS_2. Results showing that the 3-channel BL MoS_2 has the largest gain as well as I_{on}.

The simulated I_d-V_g curves in both ML and BL MoS_2 with respect to the channel number are also under the extraction of V_{th_lin} at 206 mV in L_g = 10 nm in Fig. 7(a). The results of I_d-V_g are shown under V_{ds} = 0.05 V in Fig. 7(b). About twice t_{ch} are found in BL MoS_2 compared with ML MoS_2, the magnitudes of I_{on} of BL are about twice compared with ML MoS_2 ones. Next, we illustrate the Bode plot, shown in Fig. 7(c) by considering a common source (CS) amplifier. The

TABLE II LIST OF CALCULATED ELECTRONIC PROPERTIES OF ML AND BL MoS_2, COMPARED WITH REPORTED RESULTS.

	Bandgap		Electron affinity		Effective mass	
Si	1.12 eV		4.08 eV		0.187 m_0	
ML	1.78 eV		4.26 eV		0.459 m_0	
Ref.	Expt.	1.8 [1]	**Sim.**	4.03 [14]	**Sim.**	0.51 [15] 0.45 [7]
	Sim.	1.9 [11] 1.68 [12] 1.57 [13]				
2L	1.40 eV		4.21 eV		0.608 m_0	
Ref.	Sim.	1.5 [14] 1.60 [15]	**Sim.**	4.14 [14]	**Sim.**	0.52 [15] 0.54 [16]

TABLE III LIST OF THE ML AND BL MoS_2 FREQUENCY RESPONSE OF 3DB AND UNITY GAIN F_T (HZ).

	ML 1-ch	BL 1-ch	ML 2-ch	BL 2-ch	ML 3-ch	ML 3-ch
3dB	8.27e11	1.30e12	8.96e11	1.98e12	1.13e12	1.13e12
f_T	8.73e11	9.19e11	9.09e11	8.69e11	8.90e11	8.32e11

TABLE IV LIST OF THE EXPLORED 3-CHANNEL DEVICE WITH ML AND BL MoS_2 FILMS, COMPARED WITH DIFFERENT REPORTED RESULTS.

Papers	Materials	SS(mV/dec)	DIBL(mV/dec)	I(A/μm)
This work	**MoS_2 ML**	58.0	14.1	4.76×10^{-4}
[17]		61.6	14.9	1.52×10^{-4}
[18]		70.4	42.2	4.04×10^{-4}
This work	**MoS_2 BL**	60.3	15.2	7.20×10^{-4}
[17]		64.6	28.0	1.25×10^{-3}
[18]		89.0	90.0	5.31×10^{-4}

GAA NS FET with the BL MoS_2 channel shows its well performance on the relatively larger gain compared with the ML MoS_2; especially, in the 3-channel GAA NS FET with BL MoS_2. Higher gain in 3-channel can refer to the characteristics of multi-channel, while in BL can derive in its larger m_0^* and twice t_{ch} in contrast to ML MoS_2. The frequency response in 3dB and f_T is shown in Tab. III. All the cases in ML and BL MoS_2 lie on the similar frequency response.

As shown in Fig. 7(d), the estimated DIBL and SS of ML and BL MoS_2 indicate that the BL MoS_2 has larger degradation, compared with the results of ML MoS_2 due to the larger t_{ch} as well as m_0^*. However, the values of DIBL in 1-channel has higher value than in other cases, means that the main reason cause the increase of value in DIBL is depending on the effective area of the structure. Despite the fact that BL MoS_2 performs larger value in SS, the values comparing with Si is still much smaller, which means that BL MoS_2 is still a practical device to reduce the SCE with its 2D t_{ch} and larger m_0^*. To support the reliable SS, DIBL, and I_{on} we calculate in this work for 3-channel GAA NS FET in ML and BL MoS_2, the results are also compared with other papers in [17]-[18], as listed in Tab. IV. It shows that the results in this study shows that with reasonably low SS and DIBL in this study can perform highest I_{on} comparing with other simulation results.

IV. CONCLUSIONS

In summary, we have examined DC/AC/RF characteristic of the explored multi-channel GAA NS FET with ML and BL MoS_2 films. As compared to the control sample of Si, MoS_2 devices exhibit reduced SCE. BL MoS_2 with its moderate band gap comparing with Si and ML MoS_2 as well as larger channel thickness in 2D properties comparing with ML MoS_2 can improve on the state current and voltage gain of GAA NS FETs. Despite the fabulous results shown in this work, there are still few problems that are not considered in this work, such as the contact resistance between S/D metal and MoS_2, also the effect of the device when considering different types of oxide layer. Our future work will focus on maintaining excellent results after considering the contact resistance. Also, we will compare the results of MoS_2 GAA NS FET with different types of oxide layer including Al_2O_3, and hBN.

ACKNOWLEDGMENT

This work was supported in part by the National Science and Technology Council, Taiwan, under Grant MOST 111-2221-EA49–181 and NSCT 112-2218-E-006-009-MBK; in part by the "2022 Qualcomm Taiwan Research Program (NYCU)" under Grant NAT-487835 SOW.

REFERENCES

[1] K. F. Mak et al., "Atomically thin MoS_2: a new direct-gap semiconductor," Phys Rev Lett, vol. 105, no. 13, 136805, Sep. 2010.

[2] C.-Y. Chen et al., "Electronic Structures of Monolayer Binary and Ternary 2D Materials: MoS_2, WS_2, $Mo_{1-x}Cr_xS_2$, and $W_{1-x}Cr_xS_2$ Using Density Functional Theory Calculations," Nanomaterials, vol. 13, no. 1, 68, Dec. 2022.

[3] B. Radisavljevic et al., "Single-layer MoS_2 transistors," Nature Nanotech, vol. 6, no. 3, pp. 147-150, Mar. 2011.

[4] Y.-Y. Chung et al., "First Demonstration of GAA Monolayer-MoS_2 Nanosheet nFET with 410 μA/μ m I_D at 1V V_D at 40nm gate length," in IEDM, Dec. 2022, pp. 823-826.

[5] X. Xiong et al., "Demonstration of Vertically-stacked CVD Monolayer Channels: MoS_2 Nanosheets GAA-FET with I_{on} > 700 μA/μm and MoS_2/WSe_2 CFET," in IEDM, Dec. 2021, pp. 162-165.

[6] Y. Yoon et al. "How Good Can Monolayer MoS_2 Transistors Be?," Nano Lett., vol. 11, no. 9, pp. 3768–3773, Sep. 2011.

[7] A. Pon et al., "Simulation of 2D Layered Material Ballistic FETs using a Hybrid Methodology," in IEEE EDSSC, Jun. 2019, pp. 1-3.

[8] A. Kuc et al., "Influence of quantum confinement on the electronic structure of the transition metal sulfide TS_2," Phys. Rev. B, vol. 83, no. 24, 245213, Jun. 2011

[9] K. K. H. Smithe et al., "High-Field Transport and Velocity Saturation in Synthetic Monolayer MoS_2," Nano Lett., vol. 18, no. 7, pp. 4516-4522, Jul. 2018.

[10] J.-H. Hur et al., "A theoretical modeling of photocurrent generation and decay in layered MoS_2 thin-film transistor photosensors," J. Phys. D: Appl. Phys., vol. 50, no. 6, 065105, Jan. 2017.

[11] L. Liu et al., "Performance Limits of Monolayer Transition Metal Dichalcogenide Transistors," IEEE Trans. Electron Devices, vol. 58, no. 9, pp. 3042–3047, Sep. 2011.

[12] S. Ahmad and S. Mukherjee, "A Comparative Study of Electronic Properties of Bulk MoS_2 and Its Monolayer Using DFT Technique: Application of Mechanical Strain on MoS_2 Monolayer," Graphene, vol. 03, no. 04, pp. 52-59, 2014.

[13] A. Kumar and P. K. Ahluwalia, "A first principle Comparative study of electronic and optical properties of 1H – MoS_2 and 2H – MoS_2," Mater. Chem. Phys., vol. 135, no. 2, pp. 755-761, Aug. 2012.

[14] H. Kim and H. J. Choi, "Thickness dependence of work function, ionization energy, and electron affinity of Mo and W dichalcogenides from DFT and GW calculations," Phys. Rev. B, vol. 103, no. 8, 085404, Feb. 2021.

[15] D. Wickramaratne et al., "Electronic and thermoelectric properties of few-layer transition metal dichalcogenides," J. Chem. Phys., vol. 140, no. 12, 124710, Mar. 2014.

[16] S. Yu et al., "Phase transition, effective mass and carrier mobility of MoS_2 monolayer under tensile strain," Appl. Surf. Sci., vol. 325, pp. 27–32, Jan. 2015.

[17] A. Mukhopadhyay et al., "The effect of the stacking arrangement on the device behavior of bilayer MoS_2 FETs," J. Comput Electron, vol. 20, no. 1, pp. 161–168, Feb. 2021.

[18] W. Cao et al., "2D Semiconductor FETs—Projections and Design for Sub-10 nm VLSI," IEEE Trans. Electron Devices, vol. 62, no. 11, pp. 3459–3469, Jan. 2015.